

1 **Analysis of Patient-specific Surgical Ventricular Restoration -** 2 **Importance of an Ellipsoidal Left Ventricular Geometry for** 3 **Diastolic and Systolic Function**

4
5 **Lik Chuan Lee^{1,2}, Jonathan F. Wenk³, Liang Zhong⁴, Doron Klepach^{1,2},**
6 **Zhihong Zhang¹, Liang Ge^{1,2}, Mark B. Ratcliffe^{1,2}, Tarek I. Zohdi⁵, Edward**
7 **Hsu⁶, Jose L. Navia⁷, Ghassan S. Kassab⁸ and Julius M. Guccione^{1,2}**

8 Department of Surgery¹and Bioengineering², University of California, San Francisco, CA; Department of
9 Mechanical Engineering and Surgery University of Kentucky, Lexington, KY ³; Department of Cardiology,
10 National Heart Centre Singapore⁴; Department of Mechanical Engineering, University of
11 California, Berkeley⁵; Department of Bioengineering, The University of Utah⁶; Cleveland
12 Clinic⁷; Department of Biomedical Engineering, Indiana University –Purdue University Indianapolis ⁸

16 **Author Contributions:**

17 Lik Chuan, Lee: Mathematical modeling, result analysis, manuscript writing.
18 Jonathan F. Wenk: Mathematical modeling.
19 Liang Zhong: Manuscript editing, Data collection.
20 Doron Kepach: Mathematical modeling.
21 Zhang Zhihong: Mathematical modeling.
22 Liang Ge: Result analysis.
23 Mark B. Ratcliffe: Result analysis.
24 Edward Hsu: Data collection.
25 Jose L. Navia: Data collection.
26 Tarek Zohdi: Manuscript editing.
27 Ghassan S. Kassab: Manuscript editing, result analysis.
28 Julius M. Guccione: Manuscript editing, result analysis.

29
30
31 Running head: Analysis of patient-specific SVR
32
33
34

35 *Corresponding Author:

36 Julius M. Guccione
37 UCSF/VA Medical Center (112D)
38 4150 Clement Street
39 San Francisco, CA 94121
40 Phone: 415-221-4810
41 Fax: 415-750-2181
42 Email: julius.guccione@yahoo.com

44 **Summary**

45 Surgical ventricular restoration (SVR) is a procedure designed to treat heart failure by surgically
46 excluding infarcted tissues from the dilated failing left ventricle. To elucidate and predict the effects of
47 geometrical changes from SVR on cardiac function, we created patient-specific mathematical (finite
48 element) left ventricular models before and after surgery using untagged magnetic resonance images. Our
49 results predict that the post-surgical improvement in systolic function was compromised by a decrease in
50 diastolic distensibility in patients. These two conflicting effects typically manifested as a more depressed
51 Starling relationship (stroke volume vs. end-diastolic pressure) after surgery. By simulating a restoration
52 of the left ventricle back to its measured baseline sphericity, we show that both diastolic and systolic
53 function improved. This result confirms that the increase in left ventricular sphericity commonly observed
54 after SVR (endoventricular circular patch plasty) has a negative impact and contributes partly to the
55 depressed Starling relationship. On the other hand, peak myofiber stress was reduced substantially (by
56 50%) after SVR and the resultant left ventricular myofiber stress distribution became more uniform. This
57 significant reduction in myofiber stress after SVR may help reduce adverse remodeling of the left
58 ventricle. These results are consistent with the speculation proposed in the STICH trial (20) for the neutral
59 outcome, that “the lack of benefit seen with surgical ventricular reconstruction is that benefits anticipated
60 from surgical reduction of left ventricular volume (reduced wall stress and improvement in systolic
61 function) are counter-balanced by a reduction in diastolic distensibility.”

62

63 **Keywords:** Myocardial infarction, Surgical ventricular restoration, Finite element modeling, Coronary
64 artery bypass grafting.

65

66 Word Count: 243

67 **Introduction**

68 Surgical ventricular restoration (SVR) is a procedure designed to treat heart failure by surgically
69 excluding infarcted tissues from the dilated failing left ventricle (LV). The aim of this treatment is to
70 neutralize the negative physiologic effects of dysfunctional regions in the left ventricular wall. The
71 “Surgical Treatment for Ischemic Heart Failure” (STICH) trial was conducted to assess the effectiveness
72 of SVR (35). One of the two components of the trial was to determine whether adding SVR to Coronary
73 Artery Bypass Grafting (CABG) would decrease the rate of death or hospitalization for cardiac
74 causes more than CABG alone. The clinical findings led the authors to conclude that adding SVR to
75 CABG reduces the LV volume compared to CABG alone, but this reduction is not associated with a
76 greater improvement in symptoms, exercise tolerance or a reduction in the rate of death or
77 hospitalization for cardiac causes. One speculation for these findings was that the benefits anticipated
78 from the surgical reduction of LV volume were counterbalanced by a reduction in diastolic
79 distensibility (21).

80 Although the STICH trial concluded that SVR, when performed with CABG, adds no benefits to
81 the patient, this conclusion remains controversial (7, 8, 26). Clinical studies have shown that SVR did
82 benefit patients who had myocardial infarction (3, 4, 8, 19, 24, 28) and both the European Society of
83 Cardiology and European Association for Cardio-Thoracic Surgery recommend SVR if LV volume is
84 measured, scar is identified and surgery is performed in centers with a high level of surgical expertise
85 (37). Conversely, clinical studies have also shown that stroke volume (SV) decreased after SVR (13, 22,
86 34, 39), and the decrease in size of the LV after SVR can be accompanied by an increase in LV sphericity
87 (12, 23, 39). This post-surgical increase in LV sphericity was believed to impair diastolic function (27).
88 On the other hand, the supposedly lower ventricular wall stress (based on Laplace’s law) resulting from a
89 reduction in LV size after SVR should in principle benefit patients by reducing myocardial oxygen
90 demand (30). These conflicting effects of SVR contribute, in part, to the gap in our understanding as to
91 why patients who underwent SVR did not always receive the benefits from the supposedly lower wall

92 stress. Bridging this gap requires accurate quantification of the local myofiber stress, which at present,
93 can be determined only through patient-specific mathematical modeling (38).

94 Patient-specific mathematical modeling of the effects of SVR is largely lacking and is, at best,
95 overly simplified. Many mathematical analyses of SVR have been conducted based on animal LV
96 models. For example, a mathematical model of the sheep LV by Dang et al. (10) was used to study the
97 effects of SVR alone (without CABG) on diastolic distensibility, end-systolic elastance, the Starling
98 relationship (SV versus end-diastolic pressure) and regional myofiber stress distribution. Their
99 results suggest that when compared to the remote region, SVR reduces myofiber stress in the akinetic
100 infarct and infarct borderzone. They also found that the Starling relationship was depressed after SVR.
101 However, this result is based on a sheep LV and did not address the increase in sphericity of the post-
102 surgical LV commonly found in patients. On the other hand, a recent analysis of the patient-specific
103 effects of SVR found it reduced the LV bulk wall stress and improved the LV systolic function (40). That
104 analysis was based on a local balance of forces, however, and cannot account for myofiber orientation or
105 predict myofiber stress distribution within the LV (38).

106 To elucidate the functional effects resulting from the geometrical change found in the LV after
107 SVR, we performed the first mathematical analysis on the effects of SVR using patient-specific finite
108 element (FE) LV models. These models were created using untagged magnetic resonance (MR) images
109 from the same set of patient data described in Zhong et al. (39).

110 **Material and Methods**

111 *Acquisition of magnetic resonance images*

112 The method used for magnetic resonance imaging (MRI) is detailed in Zhong et al. (40). All procedures
113 in patients were approved by our institutional review board and patient consents were obtained. The MR
114 images were de-identified. Images were obtained one to two weeks before surgery and one to two weeks
115 after surgery with a 1.5-T MRI scanner (Siemens Somatom, Erlangen, Germany). These images were

116 segmented interactively by outlining the LV endocardial and epicardial borders (excluding papillary
117 muscles and trabeculation) using CMRtools. Then, the set of LV contour points derived from the
118 segmentation process was triangulated using Rapidform[®] (INUS Technology, Inc) to reconstruct the
119 three-dimensional (3D) LV epicardial and endocardial surfaces. End-diastolic (ED) and end-systolic (ES)
120 cardiac phases were determined by visualizing the mitral valve and the aortic valve closure.

121 ***Finite element modeling***

122 We used the FE method to analyze the effects of surgery (CABG + SVR) in 12 patients (randomly
123 selected from a cohort of 40 patients). In each patient, the SVR procedure was performed using the
124 endoventricular circular patch plasty technique. Three of these 12 patients had concomitant mitral
125 regurgitation and underwent mitral valve repair surgery by means of restrictive mitral annuloplasty. A
126 multivariable general linear model analysis was performed on this patient cohort and did not detect any
127 differences between patients who received mitral valve repair surgery (MVR) and patients who did not
128 receive MVR (39). Finite element models of the LV were created by projecting a mesh between the 3D
129 endocardial and the 3D epicardial surface reconstructed from the acquired MR images (33) at early
130 diastole (Truegrid, XYZ Scientific Applications, Inc., Livermore, CA). The mesh in each LV model
131 consisted of between 2000 to 4000 trilinear 8-noded brick elements.

132 In the pre-surgery models, two distinct material regions were defined: the transmural infarct
133 region and the remote region. The infarct region was defined as the region without any relative wall
134 motion; i.e., akinesia. The remote-infarct boundary was identified by overlapping the ED and the ES
135 endocardial surface. Then, this boundary was projected transmurally onto the epicardial surface. In the
136 post-surgery models, the entire LV was assumed to be composed of a single material as there were no
137 significant overlapping regions. Residual stress was not included in the post-surgery LV models because
138 the effects were found to be negligible in a previous study (16). Rigid body motion of the LV was
139 suppressed by constraining the base from moving in the longitudinal direction and by constraining the
140 epicardial-basal edge from moving in all directions.

141 Myofiber angle distribution was assumed to vary transmurally from epicardium to endocardium
142 via a linear transition from -60° to $+60^\circ$ relative to the circumferential direction in all models (16, 29).
143 Also, we have recently obtained unpublished *ex-vivo* diffusion tensor magnetic resonance imaging
144 (DTMRI) fiber angle measurements from 5 explanted human hearts with ischemic heart failure. The
145 myofiber angle was found to vary transmurally from -42.4° (epicardium) to 35.7° (endocardium) on
146 average. To test whether the conclusions of our analysis would be impacted if these new fiber angle data
147 were used, we repeated the analysis on one LV model using these new fiber data.

148 Because pressure was not measured in the LV, the end-systolic pressure (ESP) was assumed to
149 match the measured systolic blood pressure (SBP) of individual patients. The average SBP of the
150 patients was 121 mmHg pre-surgery and 117 mmHg post-surgery. End-diastolic pressure (EDP) was
151 assumed to be 12 mmHg pre-surgery and post-surgery. The pressure was applied to the LV endocardial
152 surface. To assess the sensitivity of the pressure-volume and Starling relationship to EDP and ESP, we
153 repeated the analysis with EDP at 4 and 20 mmHg and ESP at 90% and 110% of the SBP. The sensitivity
154 of the end-systolic myofiber stress to ESP was also assessed for each case. We note that the estimation of
155 $ESP = 0.9 \times$ systolic blood pressure, as was used in many studies; e.g. in (6), falls within the range of ESP
156 used in our sensitivity analysis. Although the sensitivity analysis did not account for inter-individual
157 differences in the LV pressure (especially in EDP), it did confirm that the overall conclusions of this
158 study are not sensitive to the LV pressure assumptions.

159 Passive and active constitutive laws previously described by Guccione et al. (17, 18) were used in
160 this study (see Appendix A.1). The constitutive laws were implemented with a user-defined material
161 subroutine in LS-DYNA (Livermore Software Technology Corporation, Livermore, CA). Passive
162 stiffness of myocardial tissue was characterized by the material parameter C in the constitutive law.
163 To obtain C in each of the model, we adjusted the C -values so that the predicted LV cavity volume
164 of the FE model matched the measured end-diastolic volume (EDV). In the pre-surgery models, C
165 at infarct (C_I) was set to be ten times stiffer than that in the remote region (C_R) (36). Myocardial

166 tissue contractility in the active constitutive law was characterized by the material parameter T_{\max} , which
167 is the strength of contraction at the longest sarcomere length in the tissue. In the post-surgery FE models,
168 T_{\max} was adjusted so that the predicted LV cavity volume matched the measured end-systolic volume
169 (ESV). In the pre-surgery FE models, T_{\max} at the infarct (T_{\max_I}) and at the remote region (T_{\max_R}) were
170 optimized so that: (i) the radial strain was nominally zero at the infarct because changes in wall thickness
171 are minimal in akinesia, and (ii) the predicted LV cavity volume subjected to ESP was within $\pm 1\%$ of the
172 measured ESV. The optimization was implemented using LS-OPT (Livermore Software Technology
173 Corporation, Livermore, CA). The approach of determining active material parameters in the pre-surgery
174 models was adopted from Dang et al. (11), who have used FE models extrapolated from 2D
175 echocardiography to examine akinetic infarcts. Although our models did not physically include any post-
176 surgical implants (e.g. rigid rings, patches), the mechanical effects of these implants were, nevertheless,
177 reflected in the material parameters C and T_{\max} as they were calculated based on the MRI-measured LV
178 volumes and LV pressures that are within a physiological range.

179 Two post-surgery FE models were used to perform a study on the effects of LV sphericity, which
180 was quantified by the short-to-long-axis ratio or sphericity index (SI). The long axis dimension was
181 defined to be the apex to base distance and the short axis dimension was defined to be the maximum
182 epicardial diameter measured at the mid-LV; i.e., half way between apex and base. A large value of SI
183 indicates a more spherical LV, whereas a small value of SI indicates a more ellipsoidal LV. To simulate a
184 change in SI, a downward force was applied at the apical region to elongate the LV and a negative
185 pressure was concurrently applied at the mid-basal endocardial wall to ensure that the LV cavity volume
186 remained constant. Then, the resultant LV geometry was used as the initial “stress-free” configuration to
187 which the same fiber angle distribution was assigned. Because the myocardial material is incompressible,
188 the LV wall mass remained constant after the LV shape was modified. The downward force was not
189 present in subsequent analyses performed on the resultant LV. This force was used purely for modifying

190 the geometry of the LV. The corresponding post-surgery material parameters C and T_{\max} were used in the
 191 elongated LV models.

192 ***Pressure–volume and Starling relationships***

193 Global LV performance was quantified using the pressure-volume relationship at ED and ES, as well as
 194 by the Starling relationship. To obtain the end-diastolic pressure-volume relationship (EDPVR), the FE
 195 models were used to predict the LV EDV at different EDP ranging between 0 to 25 mm Hg. Then, the
 196 resulting pressure-volume relationship was fitted using an exponential function

$$EDP = A(e^{K_{ED} \cdot (EDV - V_{o,ED})} - 1). \quad (1)$$

197 In Eq. (1), A , $V_{o,ED}$ and K_{ED} are the fitting parameters. The parameter $V_{o,ED}$ is the LV volume at zero
 198 pressure, whereas the parameters K_{ED} and A affect the LV compliance during filling. Diastolic function
 199 was quantified using the linear slope of EDPVR at 12mmHg (E_{ED}). An improvement in diastolic
 200 function was characterized by a decrease in E_{ED} .

201 The end-systolic pressure-volume relationship (ESPVR) was obtained from the FE models by
 202 simulating the LV at different ESP, ranging from 0 to 140 mmHg. The computed LVESVs were fitted
 203 to the corresponding applied ESPs using a linear function (2, 31) as given in the next equation:

$$ESP = E_{ES}(ESV - V_{o,ES}). \quad (2)$$

204 An improvement in systolic function is characterized by an increase in the end-systolic elastance
 205 E_{ES} i.e., the gradient of the linear fit, as well as by a decrease in the volume intersection $V_{o,ES}$ of the
 206 ESPVR. The simultaneous improvement of the diastolic and systolic function translates to an
 207 improvement in SV and the Starling relationship.

208 To calculate the Starling relationship, we followed the approach used in Dang et al. (10). The
209 arterial elastance was calculated (for each case) from the measured SV, the measured EDV, the fitted
210 E_{ES} and the volume-intersect $V_{o,ES}$ of the ESPVR using Eq. (3) in Dang et al. (10). Then, the Starling
211 relationship (SV-EDP) was obtained using that same equation by substituting for these values as well as
212 for the computed EDPVR. We note that SV was not compensated in the 3 patients who had concomitant
213 mitral regurgitation and underwent mitral valve repair surgery. In the study on the effects of sphericity,
214 the arterial elastance was kept constant in each of the two groups. We have chosen here to use SV to
215 quantify the LV performance instead of ejection fraction (EF) because EF is not an independent measure
216 of LV performance after SVR (i.e., it is also sensitive to the decrease in EDV after surgery).

217

218 **Results**

219 Unless otherwise indicated, all results are reported as mean \pm standard deviation. Individual results from
220 each patient are shown in the supplemental materials.

221 ***Reconstructed left ventricular geometries and hemodynamics measurements***

222 Figure 1a shows a representation of the pre-surgery and post-surgery FE LV model from 12 patients. The
223 remote region is illustrated by the lighter region, and, in the pre-surgery models, the darker region
224 illustrates the infarct. On average, measured EDV decreased by 92.7 ± 31.0 ml (from 269.6 ± 63.5 ml to
225 176.9 ± 58.0 ml) and measured ESV decreased by 78.7 ± 30.1 ml (from 210.4 ± 62.5 ml to 131.7 ± 63.2
226 ml) after surgery. The measured heart rate of these patients increased by 6.8 ± 9.5 beats/min after surgery
227 (from 73.0 ± 8.4 beats/min to 79.8 ± 8.4 beats/min) and the corresponding cardiac output decreased by 0.6
228 ± 1.5 L/min (from 4.3 ± 1.2 L/min and 3.6 ± 1.5 L/min) after surgery. Measured systemic vascular
229 resistance index increased by 620 ± 1890 dyn.s.cm⁻⁵.m⁻² (from 2670 ± 660 dyn.s.cm⁻⁵.m⁻² to 3290 ± 1820
230 dyn.s.cm⁻⁵.m⁻²) after surgery. We also found that the LV became invariably more spherical after surgery
231 as illustrated in Fig. 1b. On average, SI increased by 30%, from 0.72 ± 0.07 to 0.98 ± 0.11 after surgery.

232 ***Predicted global LV performance***

233 Figure 2 shows a representation of the effects of surgery on the ESPVR and EDPVR found in a typical
234 patient. The bounds of the pressure-volume relationship from the sensitivity analysis are also displayed in
235 the figure. We found that ESPVR consistently shifted to the left and became steeper after surgery. On
236 average, the decrease in volume-intersect $V_{o,ES}$ after surgery was 64.1 ± 26.2 ml (from 159.2 ± 51.0 ml to
237 95.1 ± 51.3 ml), and the end-systolic elastance E_{ES} increased by more than 1.5 times (from 2.40 ± 0.81
238 mmHg/ml to 3.93 ± 2.20 mmHg/ml). Global systolic function therefore improved after surgery. This
239 result was also insensitive to the choice of ESP. For the range of ESP at 90% - 110% of the SBP, the
240 average values of $V_{o,ES}$ and E_{ES} before surgery fell within 158.4 - 160.0 ml and 2.22 - 2.57 mmHg/ml,
241 respectively. After surgery, the average values of $V_{o,ES}$ and E_{ES} for this range of ESP fell within 94.7 -
242 95.7 ml and 3.55 - 4.25 mmHg/ml, respectively.

243 Although global systolic function improved, global diastolic function to worsen after surgery and
244 the LV became less compliant during filling. Specifically, E_{ED} increased from 0.48 ± 0.15 mmHg/ml to
245 0.82 ± 0.46 mmHg/ml after surgery. For the range of EDP of 4 - 20 mmHg, the average value of E_{ED}
246 before surgery fell within 0.45 - 0.52 mmHg/ml, respectively. After surgery, the average values of E_{ED}
247 for this range of EDP fell within 0.78 - 0.92 mmHg/ml, respectively. Therefore, the decrease in global
248 diastolic function predicted by our mathematical models was also insensitive to the choice of EDP.

249 These counteracting effects found in the ESPVR and EDPVR typically translated to a more
250 depressed Starling relationship. The predicted Starling relationship remained unchanged in three patients
251 (Fig. 3a), worsened in eight patients (Fig. 3b) and improved only in one (Fig. 3c). Overall, SV decreased
252 from 59.1 ± 18.5 ml to 45.1 ± 19.1 ml, an average drop of 14 ml. Hence, the improvement gained in the
253 systolic function after surgery was negated by a worsening diastolic function in most cases.

254 ***Predicted myofiber stress distribution***

255 Figure 4a shows the effect of surgery on the LV regional myofiber stress at end-systole in a representative
256 patient. Before surgery, myofiber stress was highly inhomogeneous in the LV and was significantly
257 elevated at the thin apical region where the infarct resides. After surgery, the decrease in LV size was
258 accompanied by an increase in LV wall thickness, which led to a significant reduction in the peak
259 myofiber stress. As a result, the myofiber stress distribution became more homogeneous after surgery.
260 Figure 4b shows the peak myofiber stress in the LV before and after surgery in all 12 patients. Peak
261 myofiber stress after SVR was substantially reduced in all patients regardless of whether this comparison
262 was made with the peak myofiber stress found in the remote region of the pre-surgery LV or in the entire
263 pre-surgery LV. On average, peak myofiber stress decreased by 50% (from 141.2 ± 45.1 kPa to $70.3 \pm$
264 15.0 kPa) when compared to the remote region of the pre-surgery LV.

265 ***Predicted effects of left ventricular sphericity***

266 Figure 5 shows the effects of sphericity on the post-surgical LV model from Patient 1. Similar effects
267 were also found in Patient 2 (not shown). Figure 5a shows the geometry of the post-surgical LV as it was
268 “virtually elongated” (from the original post-surgery SI of 0.96 to an SI of 0.67) using the method
269 described in the last paragraph of the section “Finite Element Modeling”. The LV cavity volume and the
270 LV wall mass remained constant during this virtual “elongation” process. Figure 5b shows the ESPVR
271 and EDPVR with SI as a parameter. As SI decreased, or equivalently, as the LV became more elongated,
272 it became more compliant and diastolic function improved as a result. For patient 1, E_{ED} decreased
273 moderately by about 6% (from 0.96 to 0.90 mmHg/ml, respectively) with a 30% decrease in SI. Roughly
274 the same percentage of decrease in E_{ED} was also seen in patient 2 when SI decreased from 0.82 to 0.63.
275 Similar to the effects of SI on diastolic function, systolic function also improved slightly as SI decreased.
276 As SI decreased in Patient 1, E_{ES} increased slightly from 4.40 to 4.46 mmHg/ml and $V_{o,ES}$ decreased
277 from 53.1 to 50.6 ml. The same percentage of improvement in systolic function was also found in Patient

278 2 when SI decreased. The concurrent improvements in systolic and diastolic function were translated into
279 an improvement in the Starling relationship (Fig. 5c). For an EDP between 4 to 20 mmHg, SV increased
280 by about 3.5ml in both patients after a 30% reduction in SI. The diastolic and systolic function and the
281 Starling relationship did not improve after further reduction of SI.

282 All the above-mentioned results were found to be relatively insensitive to a change in fiber angle
283 distribution based on the repeated analysis (on one patient) using the recently acquired transmural linear
284 variation of fiber angle from -42.4° (epicardium) to 35.7° (endocardium).

285 **Discussion**

286 ***Effects on stroke volume, systolic and diastolic function***

287 The improvement in systolic function after SVR was compromised by a concurrent decrease in the LV
288 diastolic distensibility. This conclusion is broadly consistent with the speculation offered from the STICH
289 trial (21) and the findings from clinical studies by Tulner et al. (34) and Brinke et al. (5), who observed
290 similar effects of the surgery on EDPVR when invasive pressure-volume measurements were used
291 directly after cardiopulmonary bypass (34) and six months after surgery (5). Specifically, K_{ED} was found
292 to increase from 0.021 ± 0.009 to $0.037 \pm 0.021 \text{ ml}^{-1}$ after surgery in Tulner et al., and from 0.012 ± 0.003
293 to $0.023 \pm 0.007 \text{ ml}^{-1}$ after surgery in Brinke et al. In the clinical study by Brinke et al., end-diastolic
294 elastance E_{ED} (taken at 18 mmHg) was also found to have increased from 0.15 ± 0.08 to 0.24 ± 0.10
295 mmHg/ml after surgery. Although our prediction of E_{ED} (0.48 ± 0.15 mmHg/ml and 0.82 ± 0.46
296 mmHg/ml at pre- and post-surgery, respectively) is larger than the measurements by Brinke et al., the
297 percent increase is comparable. In terms of ESPVR, Tulner et al. found that E_{ES} improved from $1.12 \pm$
298 0.63 to 1.57 ± 0.55 mmHg/ml, whereas Brinke et al. reported no significant change in E_{ES} (1.2 ± 0.6
299 mmHg/ml) at six months after surgery. Although these values were also smaller than our prediction (2.40
300 ± 0.81 mmHg/ml and 3.93 ± 2.20 mmHg/ml before and after surgery), the percent improvement predicted
301 by our mathematical models is comparable to that reported by Tulner et al.

302 As a result of the counteracting effects of surgery on ESPVR and EDPVR, our results show that
303 the Starling relationship (or SV) was usually more depressed after surgery. This result is consistent with
304 clinical findings (13, 22, 34, 39). The average decrease in SV found from these studies was about 7.5ml
305 (compared to a decrease of 14 ml found here). In the clinical study by Brinke et al. (5), SV improved from
306 60 ± 17 to 68 ± 13 ml six months after surgery.

307 ***Effects of a more ellipsoidal LV***

308 Our results show that the decrease in SV was also accompanied by an increase in SI after surgery. This
309 finding is generally consistent with clinical findings, which show a decrease in SV (13, 22, 34, 39) and an
310 increase in sphericity (12, 40) after SVR using endoventricular circular patch plasty. In contrast to what
311 occurs after endoventricular circular patch plasty, the post-surgical LV was reported to have become more
312 ellipsoidal when SVR was performed using septal anterior ventricular exclusion or Pacopexy technique
313 (20). The values of SI reported here are larger than the values reported in Zhong et al. (40). This
314 difference is because the short axis dimension was taken to be the widest LV minor axis at the
315 endocardium based on a 4-chamber cine MRI view of the heart (40); whereas here, we have taken that
316 dimension to be the maximum diameter of the MRI-reconstructed epicardial surface at the mid-ventricle.
317 Our prediction that a decrease in SI can improve the diastolic and systolic function is also consistent with
318 the theoretical studies by Choi et al. (9) and Geerts et al. (14). In these studies, an idealized prolate LV
319 was used to show that the LV became more compliant during filling as it became more ellipsoidal (9), and
320 the left ventricular pump function was reduced in a spherical LV when compared to an ellipsoidal LV
321 (14). Given that the LV EDVs were smaller (around 80ml) in these studies than those found here (EDV =
322 176.9 ± 58 ml), the effects of sphericity appear to be size-independent, at least within the range of EDV
323 mentioned here.

324 Our results show a decrease in SI by about 30% leads to an improvement in the Starling
325 relationship of about a 3.5ml increase in SV. This result suggests that the post-surgical increase in SI
326 contributes in part to the decrease in SV found after surgery. By restoring the LV SI back to its baseline

327 value (~ 30% lower than in post-surgery SI), we showed that the decrease in SV associated with an
328 increase in sphericity cannot fully account for the 14ml post-surgical drop in SV. Therefore, it is likely
329 that there are other mechanisms contributing to the decrease in SV other than the increased sphericity
330 found after surgery.

331 ***Effects on myofiber stresses***

332 Our results show that the peak end-systolic myofiber stress decreased significantly after surgery in
333 contrast to the compromised Starling relationship. Although the bulk wall stress can be predicted using
334 Laplace's Law, prediction of the myofiber stress and its distribution within the LV requires mathematical
335 modeling (38). These results are therefore more accurate in predicting LV remodeling (1, 15, 32) and
336 regional oxygen consumption (30). Our results confirm that SVR can reduce peak myofiber stress (by
337 50% on average), which can substantially reduce left ventricular myocardial oxygen consumption, MVO₂
338 (30). On the other hand, myofiber stress distribution may also become more homogeneous as a result of a
339 more uniform ventricular wall thickness after surgery (right picture in Fig. 4a). Given that left ventricular
340 remodeling is widely believed to be initiated by an increase in both magnitude and inhomogeneity of
341 myofiber stress (1, 15, 32), the more homogeneous myofiber stress distribution found after surgery
342 suggests that SVR + CABG may attenuate further adverse remodeling of the LV. Whether SVR can
343 successfully restore myofiber stress level and distribution to those found in the normal human LV and
344 help to prevent further adverse LV remodeling will require knowledge of the myofiber stress distribution
345 in the normal human LV.

346 ***Limitations***

347 The limitations to our study are primarily due to the lack of acquired data. First, because MR images with
348 delayed gadolinium enhancement were not available, infarcted regions in the LV were determined based
349 on LV wall motion and were assumed to be transmural. As a result, other possible infarcted regions that

350 are less severe, particularly regions exhibiting hypokinesia, may have been omitted in our mathematical
351 LV models.

352 Second, we were forced to assume physiologically reasonable values of 12 mmHg as EDP for all
353 patients and the measured systolic blood pressure as ESP for individual patients because patient-specific
354 left ventricular pressure data, which requires invasive measurements using micromanometer-tipped
355 catheter, was not available. Left ventricular pressure, of course, tends to vary between patients. To
356 overcome this limitation, we conducted sensitivity analysis to test whether our conclusions are affected by
357 a variability in LV pressure. We have found that the conclusions are insensitive to a variation in LV
358 pressure.

359 ***Conclusion***

360 In this first FE analysis of the effects of CABG+SVR based on patient-specific MR images, we have
361 quantified the global and regional functional effects resulting from geometrical changes of the LV due to
362 surgery. The three main conclusions from our computational analysis are as follows. First, LV systolic
363 function improved whereas LV diastolic function worsened after SVR + CABG surgery. These
364 conflicting effects resulted in a more depressed Starling relationship after surgery. Second, post-surgical
365 increase in LV sphericity caused the stroke volume to decrease, even though this decrease is insufficient
366 to compensate for the drop in stroke volume found after surgery. Third, the peak myofiber stress
367 decreased substantially (50 %) and the myofiber stress distribution became more uniform in the LV after
368 SVR + CABG surgery. These findings are consistent with the speculation proposed in the STICH trial
369 (20) for the neutral outcome, that “the lack of benefit seen with surgical ventricular reconstruction is that
370 benefits anticipated from surgical reduction of left ventricular volume (reduced wall stress and
371 improvement in systolic function) are counter-balanced by a reduction in diastolic distensibility.” Since
372 the results we presented are based on LV models reconstructed from patients at only one clinical center
373 (Cleveland Clinic) who underwent a specific type of SVR (endoventricular circular patch plasty), they
374 may not include the effects found when SVR is performed in other centers or when the surgery is

375 performed using other variants of SVR e.g., the Pacopexy technique (20), which may confer other
376 benefits as described by Buckberg et al. (7). Since the outcome of SVR is still largely controversial, with
377 both the European Society of Cardiology and European Association for Cardio-Thoracic Surgery
378 recommending SVR (37) despite the negative outcome of Hypothesis 2 of the STICH trial (21), more
379 models of other SVR variants using patient data from other clinical centers are needed to assess patient-
380 specific efficacy of SVR.

381

382 **Acknowledgement**

383 This study was supported by the National Institutes of Health research grants: R01 HL077921 and R01
384 HL086400 (JMG) and R01 HL063348, R01 HL084431 (MBR) and HL-084529 (GSK). This support is
385 gratefully acknowledged.

386 **References**

- 387 1. Aikawa Y., Rohde L., Plehn J., Greaves S.C., Menapace F., Arnold M.O., Rouleau J.L., Pfeffer
388 M.A., Lee R.T., Solomon S.D. 2001 Regional wall stress predicts ventricular remodeling after
389 anteroseptal myocardial infarction in the Healing and Early Afterload Reducing Trial (HEART):
390 an echocardiography-based structural analysis. *Am. Heart J.* **141**, 234-242.
391
- 392 2. Aroney C.N., Herrmann H.C., Semigran M.J., William G., Boucher C.A., Fifer M.A. 1989
393 Linearity of the left ventricular end-systolic pressure volume relation in patients with severe heart
394 failure. *J. Am. Coll. Cardiol.* **14**, 127-134.
395
- 396 3. Athanasuleas C.L, Stanley A.W.H, Buckberg G.D. 1998 Restoration of contractile function
397 in the enlarged left ventricle by exclusion of remodeled akinetic anterior segment: surgical
398 strategy, myocardial protection and angiographic results. *J. Card. Surg.* **13**,418–428.
399
- 400 4. Athanasuleas C.L., Buckberg G.D., Stanley A.W.H., Siler W., Dor V., Donato M.D.,
401 Menicanti L., Oliveria S.A., Beyersdorf F., Kron I.L. et al. 2004 Surgical ventricular
402 restoration in the treatment of congestive heart failure due to post–infarction ventricular
403 dilation. *J. Am. Coll. Cardiol.* **44**, 1439–1445.
404
- 405 5. Brinke E.A., Klautz R.J., Tulner S.A., Verwey H.F., Bax J.J., SchaliJ M.J., van der Wall E.E.,
406 Versteegh M.I., Dion R.A., Steendijk P. 2010 Long-term effects of surgical ventricular
407 restoration with additional restrictive mitral annuloplasty and/or coronary artery bypass grafting
408 on left ventricular function: Six-month follow-up by pressure-volume loops. *J. Thorac.*
409 *Cardiovasc. Surg.* **140**,1338-1334.
410
- 411 6. Bourlag B.A., Lam C.S.P., Roger V.L., Rodeheffer R.J., Redfield M.M. 2009 Contractility and
412 ventricular systolic stiffening in hypertensive heart disease: Insights into the pathogenesis of heart
413 failure with preserved ejection fraction. *J. Am. Coll. Cardiol.* **54**, 410 – 418.
414
- 415 7. Buckberg G., Athanasuleas C., Conte J. 2012 Surgical ventricular restoration for the treatment of
416 heart failure. *Nat. Rev. Cardiol.* **9**, 703-716.
417
- 418 8. Buckberg G.D., Athanasuleas C.L., Wechsler A.S., Beyersdorf F., Conte J.V., Strobeck
419 J.E. 2010 The STICH trial unravelled. *Eur. J. Heart Fail.* **12**, 1024–1027.
420
- 421 9. Choi. H.F., D’hooge J., Rademakers F.E., Claus P. 2010 Influence of left ventricular shape on
422 passive filling properties and end-diastolic fiber stress and strain. *J. Biomech.* **43**, 1745–1753.
423
- 424 10. Dang A.B., Guccione J.M., Zhang P., Wallace A.W., Gorman R.C., Gorman J.H. 3rd,
425 Ratcliffe M.B. 2005 Effect of ventricular size and patch stiffness in surgical anterior
426 ventricular restoration: a finite element model study. *Ann. Thorac. Surg.* **79**, 185–193.
427
- 428 11. Dang A.B., Guccione J.M., Mishell J.M., Zhang P., Wallace A.W., Gorman R.C., Gorman
429 J.H. 3rd, and Ratcliffe M.B. 2005 Akinetic myocardial infarcts must contain contracting
430 myocytes: finite-element model study. *Am. J. Physiol. Heart Circ. Physiol.* **288**, H1844–1850.
431
- 432 12. Donato M.D., Sabatier M., Dor V., Gensini G.F, Toso A., Maioli M., Stanley A.W.H.,
433 Athanasuleas C., Buckberg G. 2001 Effects of the DOR procedure on left ventricular

- 434 dimension and shape and geometric correlates of mitral regurgitation one year after surgery.
435 *J. Thorac. Cardiovasc. Surg.* **121**, 91–96.
436
- 437 13. Donato M.D., Fantini F., Toso A., Castelvechchio S., Menicanti L., Annest L. and Burkhoff D.
438 2010 Impact of surgical ventricular reconstruction on stroke volume in patients with ischemic
439 cardiomyopathy. *J. Thorac. Cardiovasc. Surg.* **140**, 1325-1331.
440
- 441 14. Geerts L, Kerckhoffs R, Bovendeerd P, Arts T. 2003. Towards patient specific models of cardiac
442 mechanics: a sensitivity study. In: *Lecture Notes in Computer Science-Functional Imaging and*
443 *Modeling of the Heart, Proceedings*. Berlin-Heidelberg: Springer-Verlag, 81-90.
444
- 445 15. Grossman W. 1980 Cardiac hypertrophy: useful adaptation or pathologic process? *Am. J. Med.*
446 **69**, 576–584.
447
- 448 16. Guccione J.M., Moonly S.M., Wallace A.W., Ratcliffe M.B. 2001 Residual stress produced by
449 ventricular volume reduction surgery has little effect on ventricular function and mechanics: a
450 finite element model study. *J. Thorac. Cardiovasc. Surg.* **122**, 592—599.
451
- 452 17. Guccione J.M., Waldman L.K., McCulloch A.D. 1993 Mechanics of active contraction in cardiac
453 muscle: part II – cylindrical models of the systolic left ventricle. *J. Biomech. Eng.* **115**, 82–90.
454
- 455 18. Guccione J.M., Costa K.D., McCulloch A.D. 1995 Finite element stress analysis of left
456 ventricular mechanics in the beating dog heart. *J. Biomechanics* **28**, 1167–1177.
457
- 458 19. Isomura T., Hoshino J., Fukada Y., Kitamura A., Katahira S., Kondo T., Iwasaki T.,
459 Buckberg G. from the RESTORE Group. 2011 Volume reduction rate by surgical
460 ventricular restoration determines late outcome in ischemic cardiomyopathy. *Eur. J. Heart*
461 *Fail.* **13**, 423–431.
462
- 463 20. Isomura T., Horii T., Suma H., Buckberg G.D. and the RESTORE Group. 2006 Septal anterior
464 ventricular exclusion (Pacopexy) for ischemic dilated cardiomyopathy: treat form not disease.
465 *Eur. J. Cardiothorac. Surg.* **29**, S245-250.
466
- 467 21. Jones R.H., Velazquez E.J., Michler R.E., Sopko G., Oh J.K., O'Connor C.M., Hill J.A.,
468 Menicanti L., Sadowski Z., Desvigne-Nickens P., et al. 2009 Coronary bypass surgery
469 with or without surgical ventricular reconstruction. *N. Engl. J. Med.* **360**, 1705–1717.
470
- 471 22. Menicanti L., Castelvechchio S., Ranucci M., Frigiola A., Santambrogio C., Vincentiis C.,
472 Brankovic J., Donato M.D. 2007 Surgical therapy for ischemic heart failure: single-center
473 experience with surgical anterior ventricular restoration. *J. Thorac. Cardiovasc. Surg.* **134**,
474 433–441.
475
- 476 23. Menicanti L. and Donato M.D. 2002 The Dor procedure: What has changed after fifteen years of
477 clinical practice? *J Thorac. Cardiovasc. Surg.* **124**, 886-890.
478
- 479 24. Prucz R.B., Weiss E.S., Patel N.D., Nwakanma L.U., Baumgartner W.A., Conte J.V.
480 2008 Coronary artery bypass grafting with or without surgical ventricular restoration: a
481 comparison. *Ann. Thorac. Surg.* **86**, 806–814.
482
- 483 25. Retzlaff B., Voss B., Albrecht W., Lange R., Hinson A.G., Sabbah H.N., Lee R.J. and
484 Bauenrschmitt R. 2010 First in man experience with left ventricular reconstruction in patients

- 485 with systolic heart failure using a novel approach of biopolymer hydrogel implantation.
486 *Circulation*. **122**, A19753 (Abstract).
487
- 488 26. Rouleau J.L., Michler R.E., Velazquez E.J., Oh J.K., O'Conner C.M., Desvigne-Nickens P.,
489 Sopko G., Lee K.L., Jones R.H. The STICH trial: evidence-based conclusions. 2010 *Eur. J.*
490 *Heart Fail.* **12**, 1028–1030.
491
- 492 27. Salati M., Pajè A., Biasi P.D., Fundaró P., Cialfi A. and Santoli C. Severe diastolic dysfunction
493 after endoventriculoplasty. 1995 *J. Thorac. Cardiovasc. Surg.* **109**, 694-701.
494
- 495 28. Skelly N.W., Allen J.G., Arnaoutakis G.J., Weiss E.S., Patel N.D., Conte J.V. 2011 The
496 impact of volume reduction on early and long-term outcomes in surgical ventricular
497 restoration for severe heart failure. *Ann. Thorac. Surg.* **91**, 104–111.
498
- 499 29. Streeter Jr. D.D., Spotnitz H.M., Patel D.P., Ross Jr. J., Sonnenblick E.H. 1969 Fiber
500 orientation in the canine left ventricle during diastole and systole. *Circ. Res.* **24**, 339–347.
501
- 502 30. Strauer B.E., Beer K., Heitlinger K. and Höfling B. 1977 Left ventricular systolic wall stress as a
503 primary determinant of myocardial oxygen consumption: Comparative studies in patients with
504 normal left ventricular function, with pressure and volume overload and coronary heart disease.
505 *Basic Res. Cardiol.* **72**, 306-313.
506
- 507 31. Suga H., Sagawa K. and Shoukas A.A. 1973 Load independence of the instantaneous pressure-
508 volume ratio of the canine left ventricle and effects of epinephrine and heart rate on the ratio.
509 *Circ. Res.* **32**, 314-322.
510
- 511 32. Sutton M.G., Sharpe N. 2000 Left ventricular remodeling after myocardial infarction:
512 pathophysiology and therapy. *Circulation* **101**, 2981-2988.
513
- 514 33. Sun K., Stander N., Jhun C-S., Zhang Z., Suzuki T., Wang G-Y., Saeed M., Wallace A.W.,
515 Tseng E.E., Baker A.J., Saloner D., Einstein D.R., Ratcliffe M.B., Guccione J.M. 2009 A
516 computationally efficient formal optimization of regional myocardial contractility in a sheep
517 with left ventricular aneurysm. *J. Biomech. Eng.* **131**, 111001–1 –111001–10.
518
- 519 34. Tulner S.A.F., Steendijk P., Klautz R.J.M., Bax J.J., Schalij M.J., van der Wall E.E., Dion
520 R.A.E. 2006 Surgical ventricular restoration in patients with ischemic dilated cardiomyopathy:
521 evaluation of systolic and diastolic ventricular function, wall stress, dyssynchrony, and
522 mechanical efficiency by pressure–volume loops. *J. Thorac. Cardiovasc. Surg.* **132**, 610–620.
523
- 524 35. Velazquez E.J., Lee K.L., O'Connor C.M., Oh J.K., Bonow R.O., Pohost G.M., Feldman
525 A.M., Mark D.B., Panza J.A., Sopko G. et al. 2007 The rationale and design of the surgical
526 treatment for ischemic heart failure (STICH) trial. *J. Thorac. Cardiovasc. Surg.* **134**, 1540–
527 1547.
528
- 529 36. Walker J.C., Ratcliffe M.B., Zhang P., Wallace A.W., Fata B., Hsu E.W., Saloner D.,
530 Guccione J.M. 2005 MRI based finite element analysis of left ventricular aneurysm. *Am. J.*
531 *Physiol. Heart. C.* **289**, H692–700.
532
- 533 37. Wijns W., Kolh P., Danchin N., Di Mario C., Falk V., Folliguet T., Garg S., Huber K., James S.,
534 Knuuti J. et al. 2010 Guidelines on myocardial revascularization. *Eur. Heart J.* **31**, 2501-2555.
535

- 536 38. Yin F.C. 1982 Ventricular wall stress. *Circ. Res.* **49**, 829-842.
537
- 538 39. Zhong L., Sola S., Tan R.S., Le T.T., Ghista D.N., Kurra K., Navia J.L., Kassab G.S. 2009
539 Effects of surgical ventricular restoration on left ventricular contractility assessed by a novel
540 contractility index in patients with ischemic cardiomyopathy. *Am. J. Cardiol.* **103**, 674–679.
541
- 542 40. Zhong L., Su Y., Gobeawan L., Sola S., Tan R.S., Navia J.L., Ghista D.N., Chua T.,
543 Guccione J.M., Kassab G.S. 2011 Impact of surgical ventricular restoration on ventricular
544 shape, wall stress, and function in heart failure patients. *Am. J. Physiol. Heart Circ. Physiol.*
545 **300**, H1653–H1660.

546 **Figure Captions**

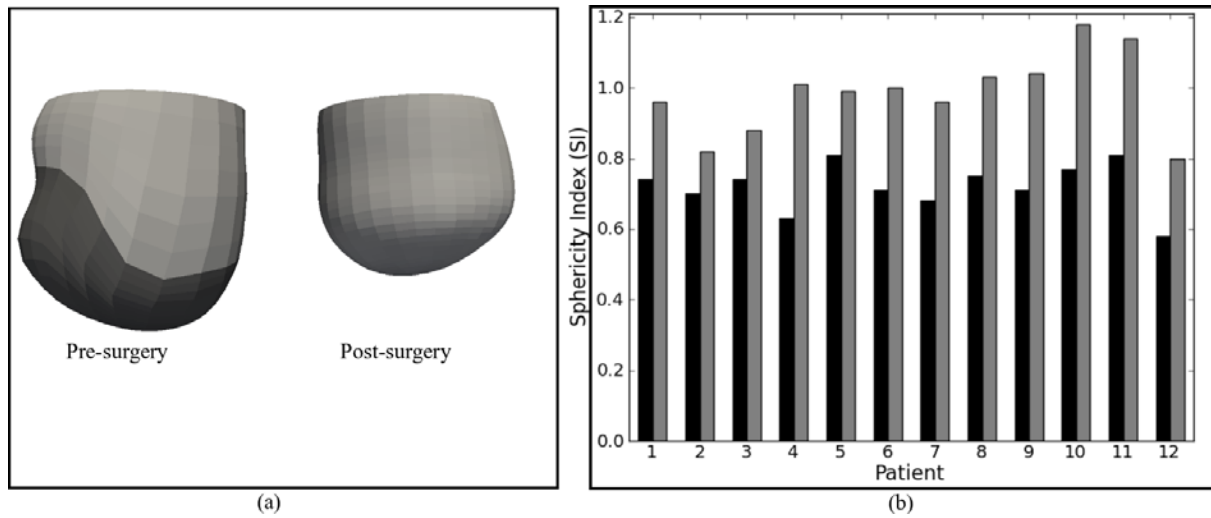
547 **Figure 1:** (a) Representative finite element LV model taken from Patient 1 pre (left) and post
548 (right) surgery. In the pre-surgery models, dark and light regions define the infarct and
549 the remote region, respectively. (b) Sphericity index (SI) of the 12 patients before
550 surgery (dark color bars) and after surgery (light color bars).

551
552 **Figure 2:** End-diastolic pressure-volume relationship (EDPVR) and end-systolic pressure-
553 volume relationship (ESPVR) after surgery (Patient 1). Black line: Pre-surgery. Grey
554 line: Post-surgery. Line type indicates the pressure-volume relationships resulting
555 from the different prescribed values of ESP and EDP. Dotted line: EDP = 4 mmHg
556 and ESP = 90% of SBP. Solid line = 12 mmHg and ESP = SBP. Dot-dash line: EDP =
557 20 mmHg and ESP = 110% of SBP.

558
559 **Figure 3:** Representative Starling relationship from three patients showing (a) no significant
560 changes (Patient 1), (b) worsening (Patient 2), (c) improvement after surgery (Patient
561 4). Dotted line: pre-surgery. Solid line: post-surgery. Bounds of the predicted Starling
562 relationship are shown as the red region for pre-surgery and as the blue region for
563 post-surgery. These bounds were calculated from the EDPVR and ESPVR obtained by
564 assuming an EDP of 4 and 20mmHg and an ESP of 90% and 110% of the systolic
565 blood pressure.

566 **Figure 4:** (a) Representative end-systolic myofiber stress distribution taken from Patient 1. The
567 left picture shows the predicted regional myofiber stress in the pre-surgery LV. The
568 right picture shows the stress in the more spherical post-surgery LV. (b) Peak end-
569 systolic myofiber stress of the 12 patients before and after surgery. Black, blue and
570 grey color bars indicate peak stress in the entire pre-surgery LV, in the pre-surgery
571 LV's remote region and in the entire post-surgery LV, respectively. Error bars show
572 the bounds of the peak myofiber stress when ESP was varied between 90% and 110%
573 of the SBP.

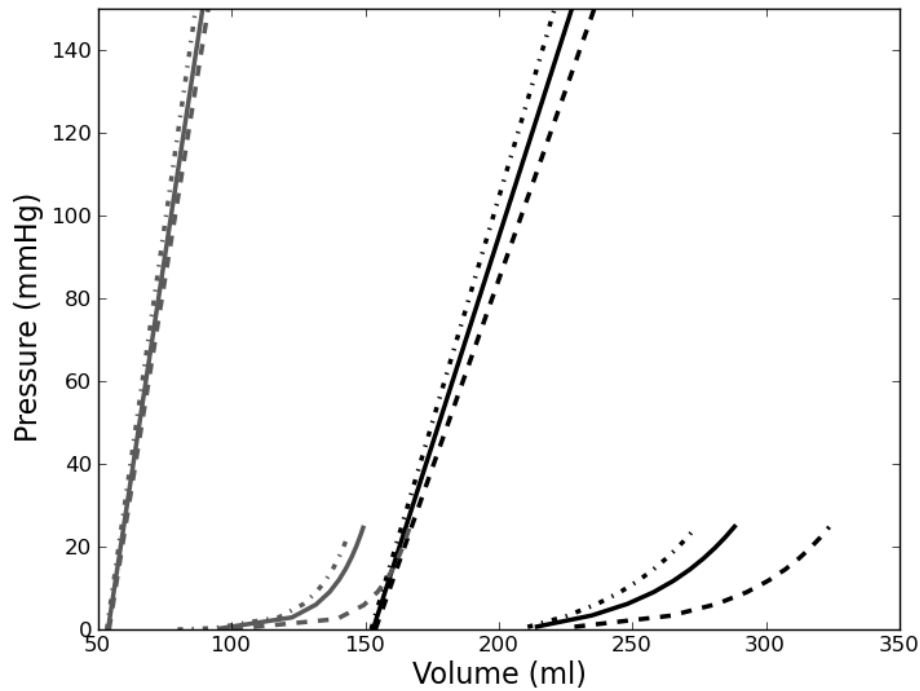
574 **Figure 5:** (a) LV with decreasing sphericity index (SI) from left to right. The original LV of
575 Patient 1 after surgery is shown on the left panel and the "virtually elongated" LVs are
576 on the center and right panel. (b) Effects of LV SI on EDPVR and ESPVR. (c) The
577 effects of LV SI on the Starling relationship. Dotted line (SI = 0.96), dashed line (SI =
578 0.78) and solid line (SI = 0.67).

579 **List of figures**

580

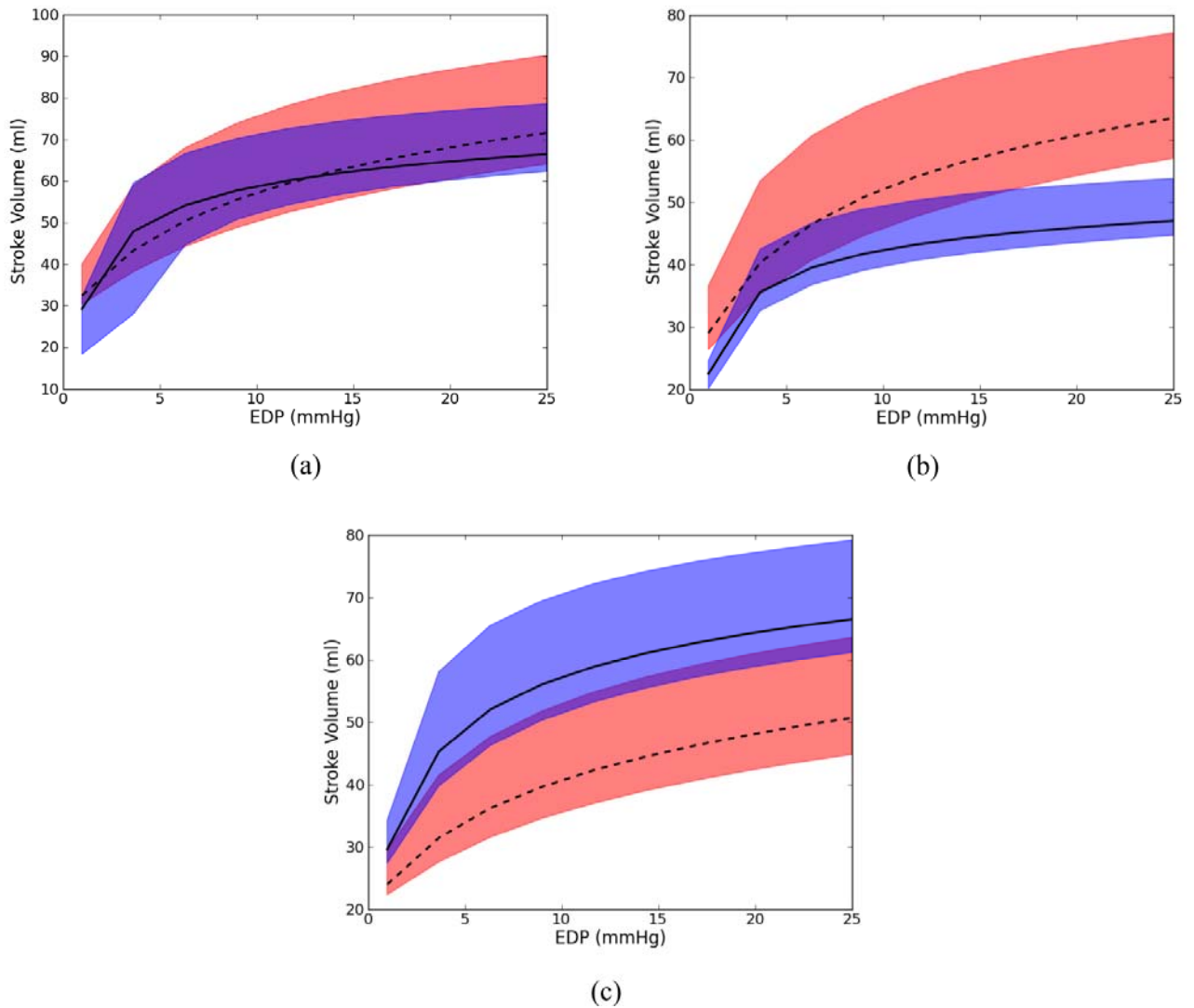
581 **Figure 1:** (a) Representative finite element LV model taken from Patient 1 pre (left) and post
582 surgery. In the pre-surgery models, dark and light regions define the infarct and the remote region,
583 respectively. (b) Sphericity index (SI) of the 12 patients before surgery (dark color bars) and after surgery
584 (light color bars).

585



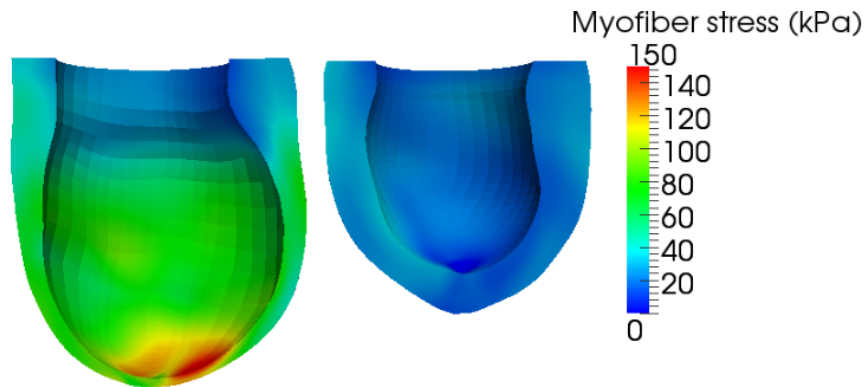
586

587 **Figure 2:** End-diastolic pressure-volume relationship (EDPVR) and end-systolic pressure-volume
588 relationship (ESPVR) after surgery (Patient 1). Black line: Pre-surgery. Grey line: Post-surgery. Line type
589 indicates the pressure-volume relationships resulting from the different prescribed values of ESP and
590 EDP. Dotted line: EDP = 4 mmHg and ESP = 90% of SBP. Solid line = 12 mmHg and ESP = SBP. Dot-
591 dash line: EDP = 20 mmHg and ESP = 110% of SBP.

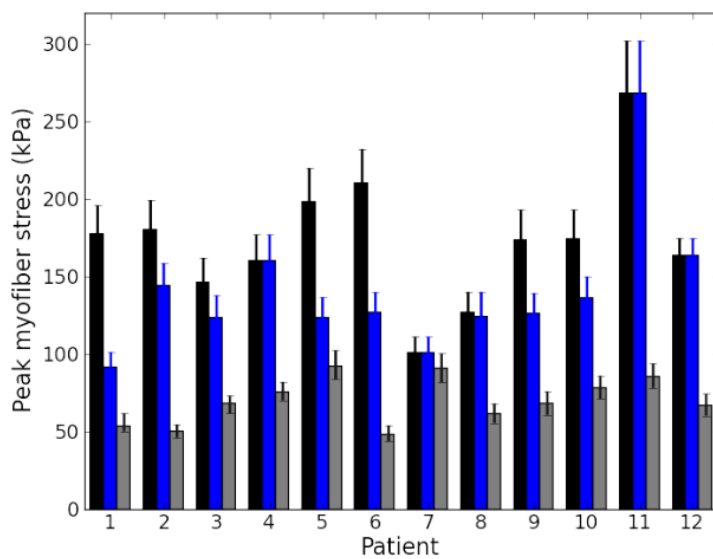


592

593 **Figure 3:** Representative Starling relationship from three patients showing (a) no significant changes
 594 (Patient 1), (b) worsening (Patient 2), and (c) improvement after surgery (Patient 4). Dotted line: pre-
 595 surgery. Solid line: post-surgery. Bounds of the predicted Starling relationship are shown as the red
 596 region for pre-surgery and as the blue region for post-surgery. These bounds were calculated from the
 597 EDPVR and ESPVR obtained by assuming an EDP of 4 and 20mmHg and an ESP of 90% and 110% of
 598 the systolic blood pressure.



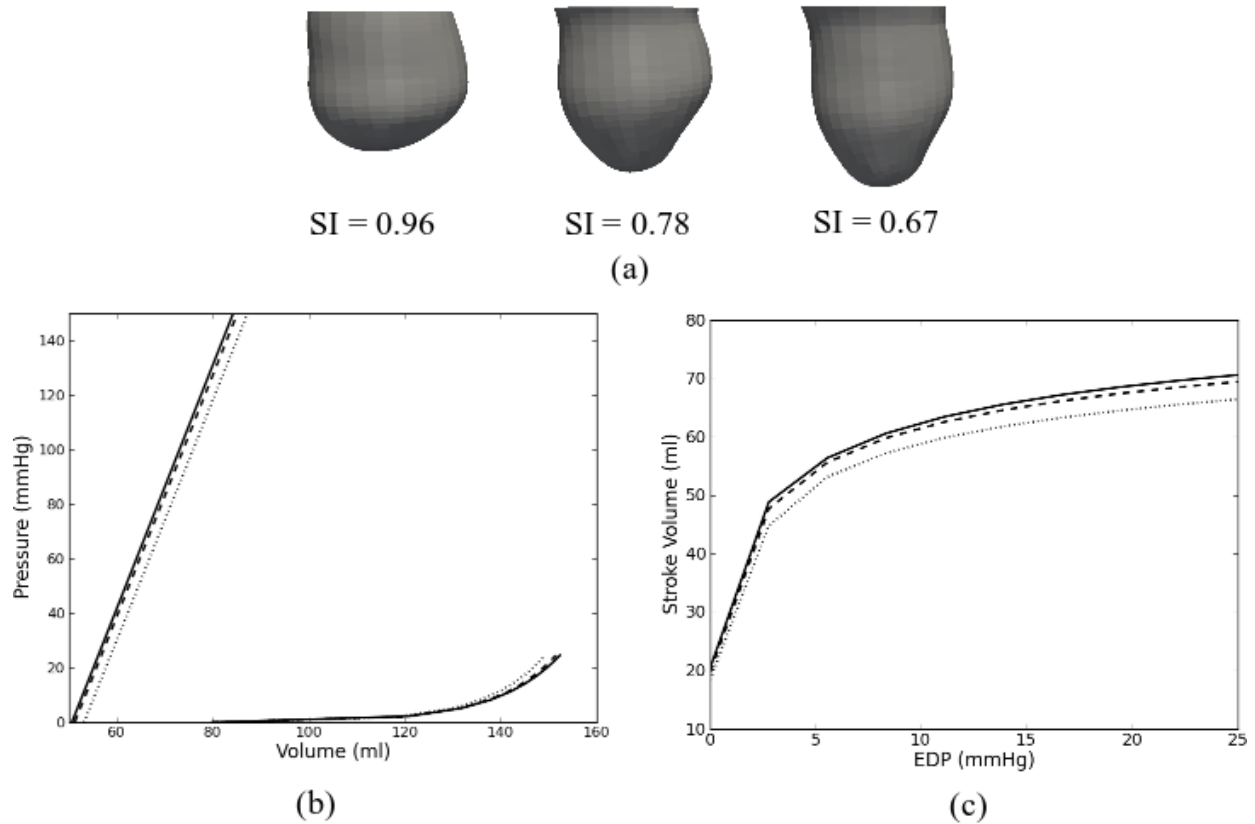
(a)



(b)

599

600 **Figure 4:** (a) Representative end-systolic myofiber stress distribution taken from Patient 1. The left
 601 picture shows the predicted regional myofiber stress in the pre-surgery LV. The right picture shows the
 602 stress in the more spherical post-surgery LV. (b) Peak end-systolic myofiber stress of the 12 patients
 603 before and after surgery. Black, blue and grey color bars indicate peak stress in the entire pre-surgery LV,
 604 in the pre-surgery LV's remote region and in the entire post-surgery LV, respectively. Error bars show
 605 the bounds of the peak myofiber stress when ESP was varied between 90% and 110% of the SBP.



606

607 **Figure 5:** (a) LV with decreasing sphericity index (SI) from left to right. The original LV of Patient 1
 608 after surgery is shown on the left panel and the “virtually elongated” LVs are on the center and right
 609 panel. (b) Effects of LV SI on EDPVR and ESPVR. (c) The effects of LV SI on the Starling relationship.
 610 Dotted line (SI = 0.96), dashed line (SI = 0.78) and solid line (SI = 0.67).

611 **Appendix A.1: Constitutive law of the myocardial tissue**

612 Nearly incompressible, transversely isotropic, hyperelastic constitutive laws for passive (18) and active
 613 myocardium (17) were used to model diastolic filling and active contraction. Passive material properties
 614 were represented by the strain energy function:

$$615 \quad W = \frac{C}{2} \left\{ \exp \left[b_f E_{11}^2 + b_t (E_{22}^2 + E_{33}^2 + E_{23}^2 + E_{32}^2) + b_{fs} (E_{12}^2 + E_{21}^2 + E_{13}^2 + E_{31}^2) \right] - 1 \right\}, \quad (\text{A.1})$$

616 where E_{11} is fiber strain, E_{22} is cross-fiber strain, E_{33} is radial strain, E_{23} is shear strain in the transverse
 617 plane, and E_{12} and E_{13} are shear strain in the fiber-cross fiber and fiber-radial planes, respectively. Values
 618 for the material constants b_f , b_t , and b_{fs} were obtained from large animal studies and have values 49.25,
 619 19.25 and 17.44 respectively (33). The material constant C was adjusted until the LV end-diastolic
 620 volumes matched the experimentally measured values as described in the main text.

621 Active contraction was modeled by defining the total stress as the sum of the passive stress
 622 derived from the strain energy function W and an active fiber directional component, \mathbf{T}_0 , which is a
 623 function of time, t , peak intracellular calcium concentration, Ca_0 , sarcomere length, l , and maximum
 624 isometric tension achieved at the longest sarcomere length, T_{\max} (17) i.e.

$$625 \quad \mathbf{S} = p J \mathbf{C}^{-1} + 2 J^{-2/3} \text{Dev} \left(\frac{\partial \tilde{W}}{\partial \tilde{\mathbf{C}}} \right) + \mathbf{T}_0(t, Ca_0, l, T_{\max}), \quad (\text{A.2})$$

626 In Eq. (A.2), \mathbf{S} is the second Piola-Kirchoff stress tensor, p is the hydrostatic pressure introduced as the
 627 Lagrange multiplier needed to ensure incompressibility, J is the Jacobian of the deformation gradient
 628 tensor, \mathbf{C} is the right Cauchy-Green deformation tensor, $\tilde{\mathbf{C}}$ is the deviatoric decomposition of \mathbf{C} (i.e.
 629 $\mathbf{C} = J^{2/3} \tilde{\mathbf{C}}$), \tilde{W} is the deviatoric contribution of the strain energy function W given in Eq. (A.1) and Dev is
 630 the deviatoric projection operator defined as

$$631 \quad \text{Dev}(\bullet) = (\bullet) - \frac{1}{3} \left([\bullet] : \mathbf{C} \right) \mathbf{C}^{-1}. \quad (\text{A.3})$$

632 Assumption of near incompressibility of the myocardium also requires the decoupling of the strain energy
 633 function W into its dilational U and deviatoric components \tilde{W} , i.e.

$$634 \quad W = U(J) + \tilde{W}(\tilde{\mathbf{C}}). \quad (\text{A.4})$$

635 The active fiber-directed stress component is defined by a time-varying elastance model, which at end-
 636 systole, is reduced to

$$637 \quad T_0 = \frac{1}{2} T_{\max} \frac{Ca_0^2}{Ca_0^2 + ECa_{50}^2} \left(1 - \cos \left(\frac{0.25}{m l_R \sqrt{2 E_{11} + 1} + b} + 1 \right) \pi \right). \quad (\text{A.5})$$

638 In Eq. (A.5), m and b are material constants, and ECa_{50} is the length-dependent calcium sensitivity given
 639 by

$$640 \quad ECa_{50} = \frac{(Ca_0)_{\max}}{\sqrt{\exp \left[B \left(l_R \sqrt{2 E_{11} + 1} - l_0 \right) \right] - 1}}, \quad (\text{A.6})$$

641 where B is a constant, $(Ca_0)_{\max}$ is the maximum peak intracellular calcium concentration, l_0 is the
 642 sarcomere length at which no active tension develops and l_R is the stress-free sarcomere length. Material
 643 constants for active contraction were taken to be (33): $Ca_0 = 4.35 \mu\text{mol/L}$, $(Ca_0)_{\max} = 4.35 \mu\text{mol/L}$, $B =$
 644 $4.75 \mu\text{m}^{-1}$, $l_0 = 1.58 \mu\text{m}$, $m = 1.0489 \text{ sec } \mu\text{m}^{-1}$, $b = -1.429 \text{ sec}$, and $l_R = 1.85 \mu\text{m}$. Based on biaxial
 645 stretching experiments, cross-fiber, in-plane active stress equivalent to 40% of that along the myocardial
 646 fiber direction was also added. Determination of the patient-specific material parameter T_{\max} is described
 647 in the main text.